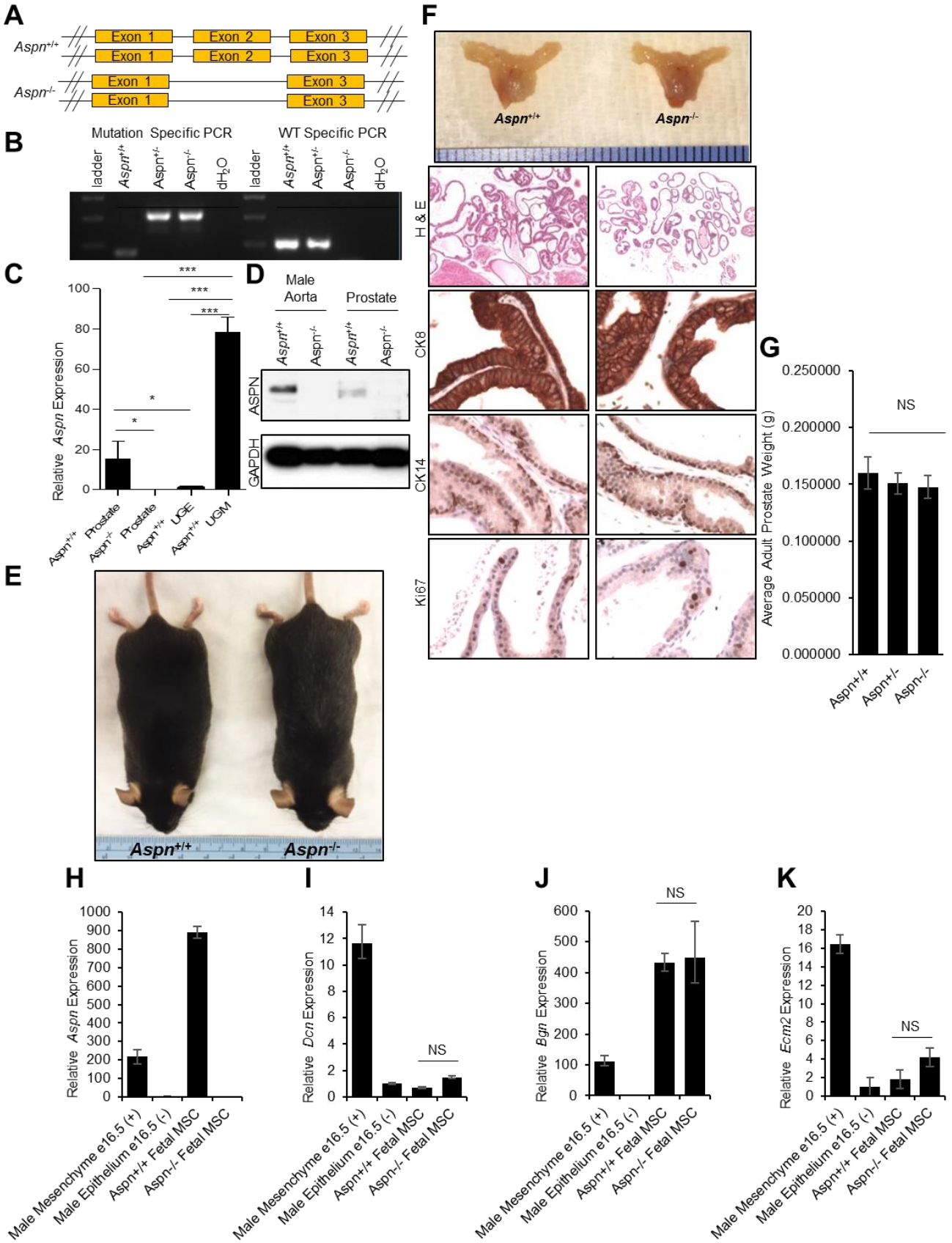

Supplementary Figure S1. Comparison of *Aspn*$^{+/+}$ and *Aspn*$^{-/-}$ mice. A, Targeting schematic for the generation of *Aspn*$^{-/-}$ mice (B6J-*Aspn*^{tm1Lex}/Mmucd). B, Wild-type (WT) and mutation specific PCR for genotyping *Aspn*$^{-/-}$ mice. C, *Aspn* expression as determined by qRT-PCR in *Aspn*$^{+/+}$ and *Aspn*$^{-/-}$ prostates compared to male *Aspn*$^{+/+}$ UGE (E) and UGM (M) at e16.5. Statistical analyses performed using one way ANOVA with Tukey multiple comparison (mean ± SEM; **P*≤0.05, ****P*≤0.001; n=3). D, ASPN expression as determined by immunoblotting of *Aspn*$^{+/+}$ and *Aspn*$^{-/-}$ prostates and aorta. J, *Aspn*$^{+/+}$ and *Aspn*$^{-/-}$ mice at 6 months of age backcrossed at least 9 generations to C57BL/6J. F, *Aspn*$^{+/+}$ and *Aspn*$^{-/-}$ prostates examined by H&E and IHC for CK8, CK14, and Ki67. G, Comparison of *Aspn*$^{+/+}$ and *Aspn*$^{-/-}$ prostate weight. H-K, Relative *Aspn, Dcn, Bgn, and Ecm2* expression as determined by qRT-PCR in UGM, UGS, *Aspn*$^{+/+}$ MSCs, and *Aspn*$^{-/-}$ MSCs. Statistical analyses performed using one-way ANOVA with Tukey multiple comparison (mean ± SEM; NS = Not Significant).

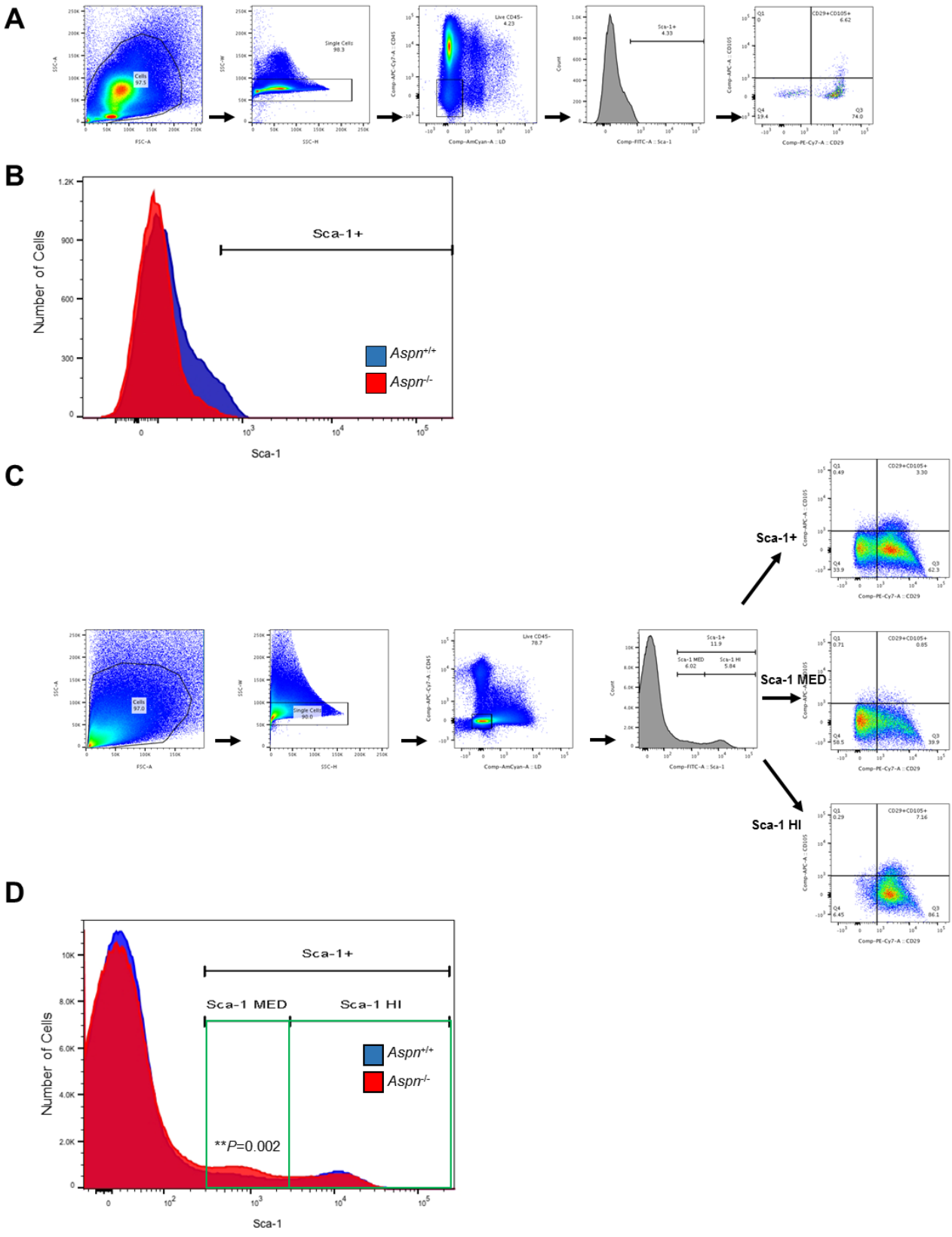

Supplementary Figure S2. Representative gating of murine adult bone marrow and prostate MSCs by flow cytometry. A, B, Gating for CD45-, CD29+, CD105+, and Sca-1+ MSCs in the bone marrow. C, D, Gating for CD45-, CD29+, CD105+, and Sca-1+ MSCs in the prostate (including Sca1^{med} and Sca1^{hi}).

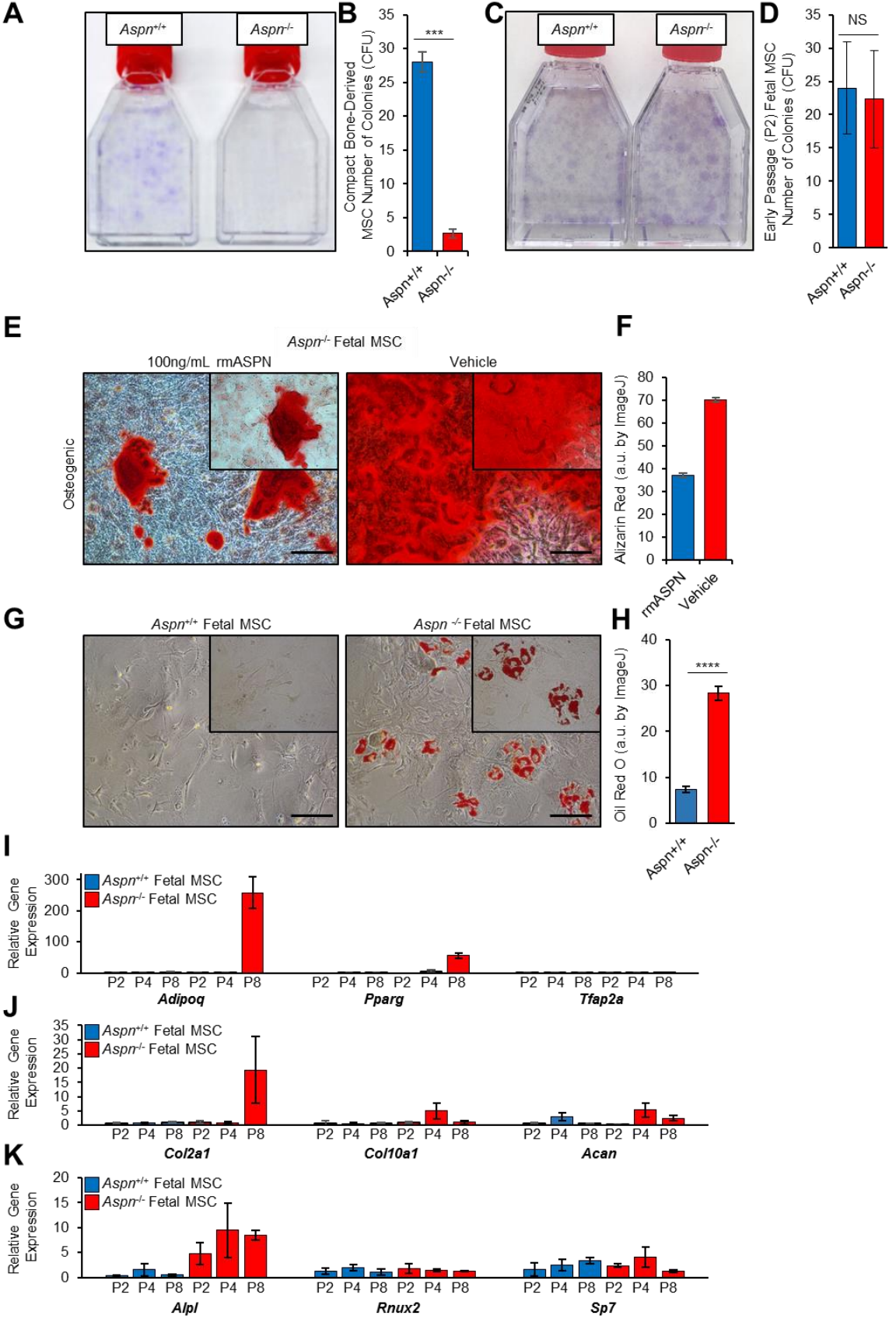

Supplementary Figure S3. ASPN restricts MSC differentiation. A, *Aspn*$^{+/+}$ and *Aspn*$^{-/-}$ adult compact bone-derived MSCs were isolated and then plated at equal densities for CFU assays. Displayed are the average number of colonies formed per 5 x 10^4 cells plated. Statistical analyses performed using Student's t-test (mean ± SEM; ***$P \leq 0.001$; n≥2). C, D, Early passage (P2) *Aspn*$^{+/+}$ and *Aspn*$^{-/-}$ fetal MSCs were plated at equal densities for CFU assays. Displayed are the average number of colonies formed per 1 x 10^4 cells plated. Statistical analyses performed using Student's t-test (mean ± SEM; NS = not significant; n≥2). E, F, *Aspn*$^{-/-}$ fetal MSCs were cultured in osteogenic-inducing media plus vehicle or 100 ng/mL of recombinant mouse ASPN**.** G-K, ASPN regulates MSC differentiation. G, H, *Aspn*$^{+/+}$ and *Aspn*$^{-/-}$ fetal MSCs were cultured in normal media for 8 passages (P8) and then stained for Oil Red O. Staining was quantified using ImageJ (n=3). I-K, Expression of (I) adipogenic, (J) chondrogenic, and (K) osteogenic differentiation-induced genes in *Aspn*$^{+/+}$ and *Aspn*$^{-/-}$ fetal MSCs at P2, P4, and P8 as determined by qRT-PCR (n≥3).

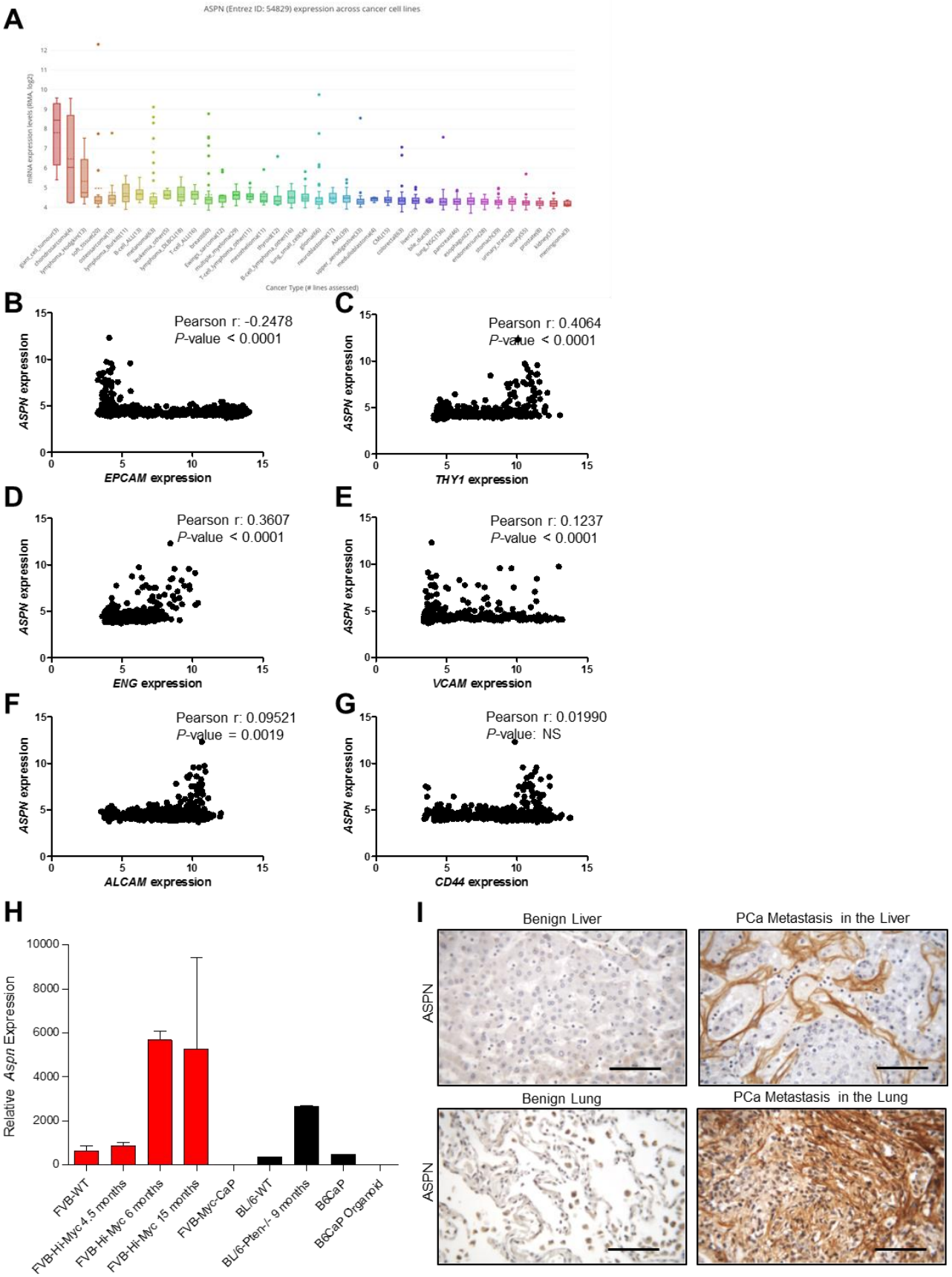

Supplementary Figure S4. ASPN expression in human cancer cell lines is correlated with MSC markers. A, *ASPN* expression in human cancer cell lines (n = 1062), grouped by cancer type. B, Correlation of *ASPN* expression with *EPCAM* expression, an epithelial-derived cell marker, in cancer cell lines. C-G, Correlation of *ASPN* expression with the expression of human MSC markers, including *THY1* (C), *ENG* (D), *VCAM* (E), *ALCAM* (F), and *CD44* (G) in cancer cell lines. Cancer cell line expression data obtained from the Broad Institute's Cancer Cell Line Encyclopedia [50]. Box plot in (A) courtesy of Plotly. Statistical analyses in B-G performed using Pearson correlation coefficient. H, Relative Aspn expression in mouse models of prostate cancer including Hi-Myc (FVB), *Pten*$^{-/-}$ (C57/BL6J), and B6CaP (C57/BL6J) as measured by qRT-PCR of whole tissue. I, ASPN expression in benign tissue and metastatic prostate cancer as measured by IHC (black bar = 100 μM).

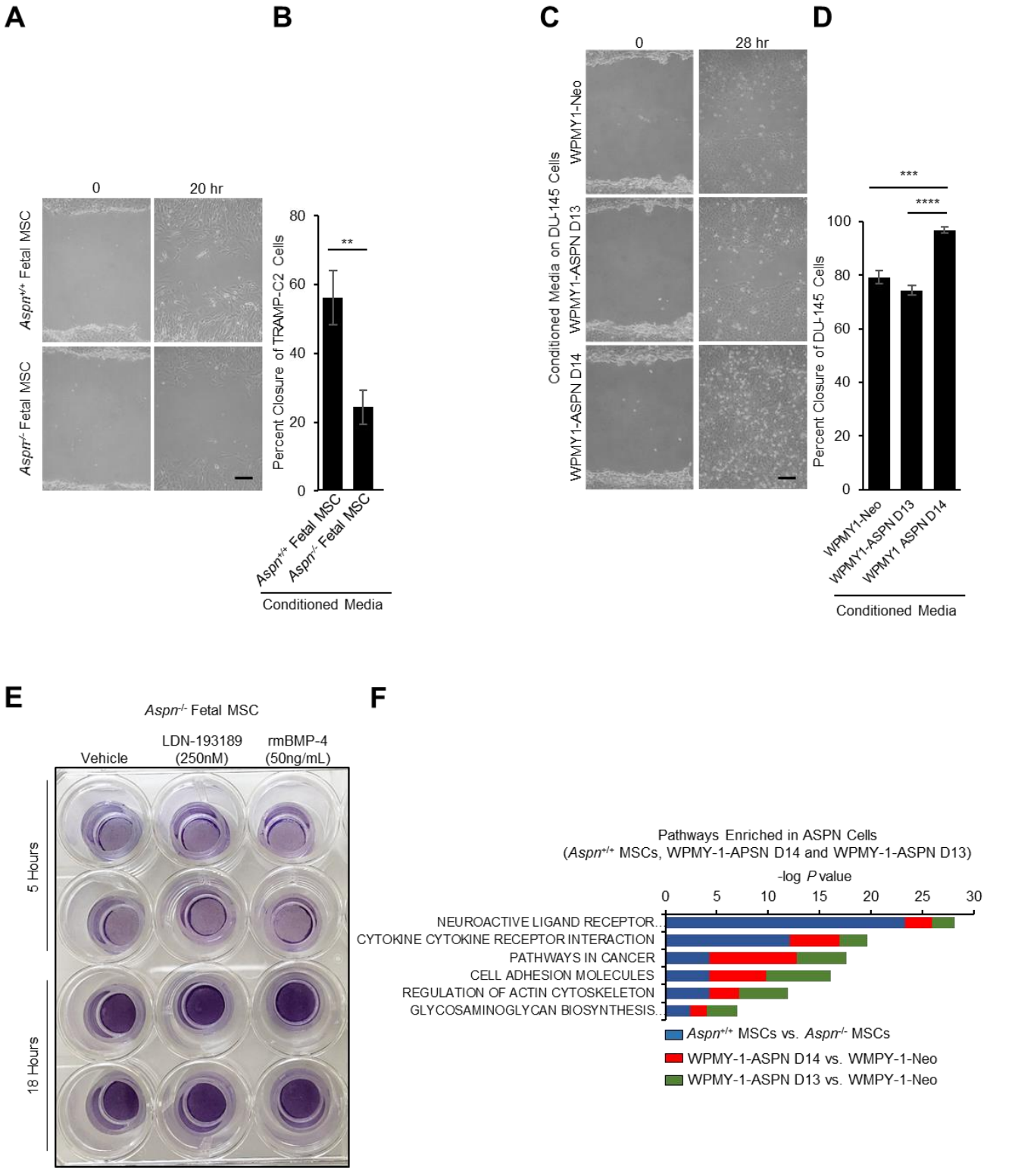

Supplementary Figure S5. ASPN increases cancer cell migration. A, B, Migration of TRAMP-C2 cells in conditioned media from *Aspn*$^{+/+}$ and *Aspn*$^{-/-}$ fetal MSCs as determined by scratch assay. Statistical analyses performed using Student's t-test (mean ± SEM; $^{**}P \leq 0.01$; n=3 independent MSCs). C, D, Migration of DU145 cells in conditioned media from WPMY-1-Neo, WPMY-1-ASPN D13, and WPMY-1-ASPN D14. Statistical analyses performed using one-way ANOVA with Tukey multiple comparison (mean ± SEM; $^{***}P \leq 0.001$, $^{****}P \leq 0.0001$; n≥9). E, Migration of *Aspn*$^{-/-}$ fetal MSCs treated with vehicle, recombinant mouse BMP-4 (50 ng/mL) or LDN-193189 (250 nM) as determined by transwell assay. F, KEGG pathway analysis in ASPN cells (*Aspn*$^{+/+}$ fetal MSCs, WPMY-1-ASPN D14, WPMY1-ASPN D13) compared to ASPN deficient/low cells (*Aspn*$^{-/-}$ and WPMY-1-Neo).

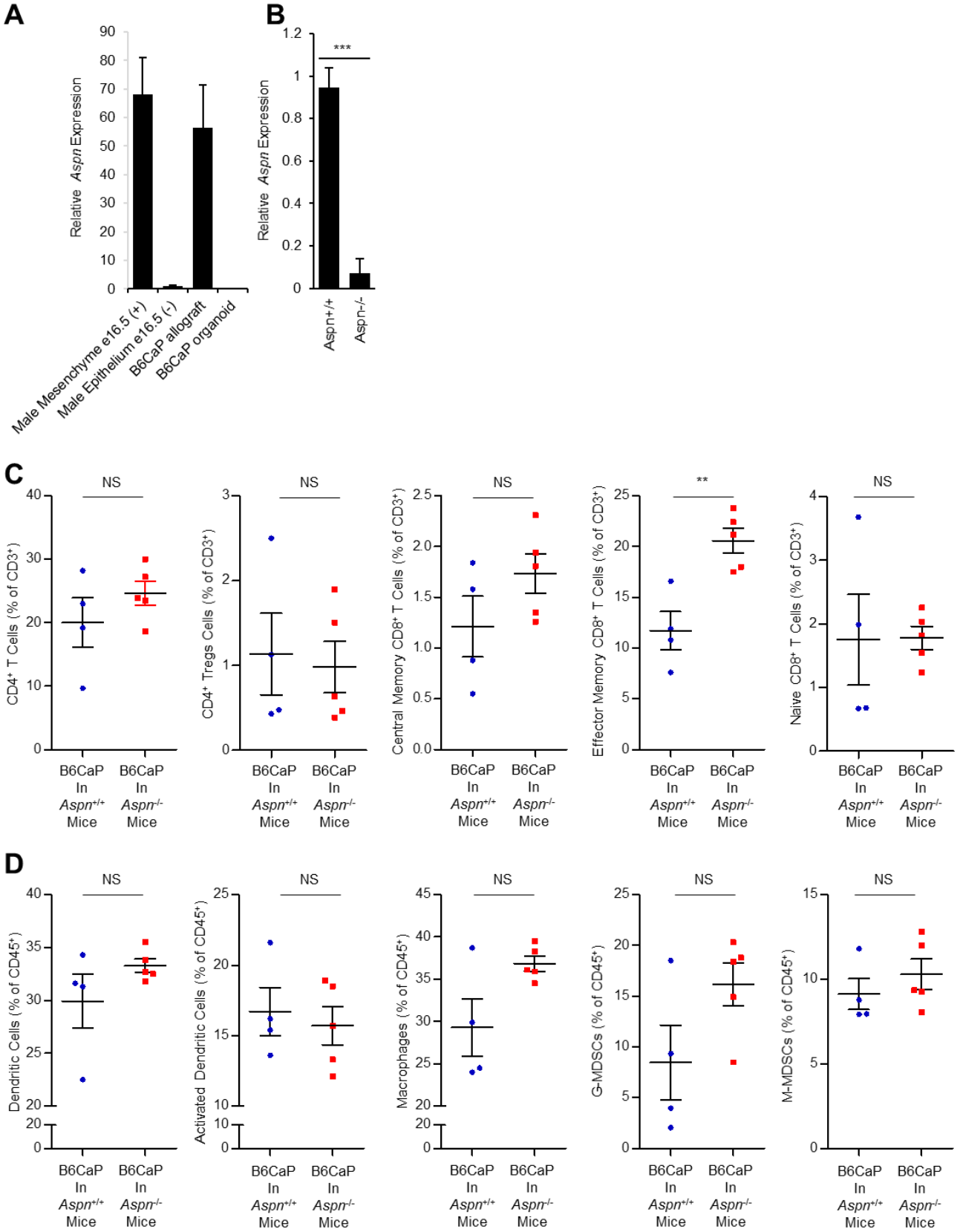

Supplementary Figure S6. *Aspn* expression in B6CaP allografts and organoids. A, Relative *Aspn* gene expression in B6CaP allograft and organoids as measured by qRT-PCR and compared to male fetal prostate mesenchyme and epithelia (n=3). B, Relative *Aspn* expression in B6CaP subcutaneous allografts at resection in *Aspn*$^{+/+}$ and *Aspn*$^{-/-}$ mice as determined by qRT-PCR. Statistical analyses performed using Student's t-test (mean ± SEM; ***$P \leq 0.001$; n≥3). C, Lymphoid cells in B6CaP subcutaneous allografts at resection in *Aspn*$^{+/+}$ and *Aspn*$^{-/-}$ mice. Tregs (CD4$^+$Foxp3$^+$), central memory CD8 (CD8$^+$, CD44$^+$, CD62L$^+$), effector memory CD8 (CD8$^+$, CD44$^+$, CD62L$^-$), naïve CD8 (CD8$^+$, CD44$^-$, CD62L$^+$). D, Myeloid cells in B6CaP subcutaneous allografts at resection in *Aspn*$^{+/+}$ and *Aspn*$^{-/-}$ mice. Dendritic Cells (CD11b$^+$, CD11c$^+$), activated dendritic cells (CD11b$^+$, CD11c$^+$, MHCII$^+$), macrophages (CD11b$^+$, F4/80$^+$), G-MDSCs (CD11b$^+$, Ly6G$^+$), M-MDSCs (CD11b$^+$, Ly6C$^+$).